

# Thermoelastic Deformation of Thin-Shell Deployable Booms

John Pederson\*, Alexandra Haraszti†, and Sergio Pellegrino‡  
Graduate Aerospace Laboratories, California Institute of Technology, Pasadena, CA

**Large lightweight booms experience thermally induced deformations on-orbit. Deflection and temperature profiles of a popular deployable geometry with desirable bending stiffness (thin-shell cylindrical section) are observed experimentally under radiant heating in a vacuum chamber, as well as predicted via multiphysics simulation. Deflection and temperature plots exhibit behavior surprising for the simple geometry, and even suggest future improvements in both modeling areas.**

## I. Introduction

To fit in current rocket fairings, large structures for space applications (e.g. solar panels and antennae) must be deployable and lightweight. The structural elements forming the backbone of these structures require strong and lightweight boom geometries; of these, the tape spring, a cylindrical thin shell with open section, creates a coilable boom that is stiff in bending [1]. Steel tape springs are a common choice for satellite antennae (not to mention the ubiquitous steel tape measure), while ultrathin composite tape springs offer similar stiffness with lighter weight. In the vacuum of space, under radiant heat from the sun, lightweight booms experience rapid temperature changes and gradients; thermal expansion / contraction within the structure can then cause significant deformations [2]. These deflections tend to inhibit accurate structural geometry, disturb spacecraft pointing, and contribute to material fatigue – all of which have afflicted almost two dozen space missions over the last sixty years [3]. As such, the deflection response of steel tape springs under radiant heating was investigated; careful multiphysics simulations, validated by experimental measurements, were carried out to understand the surprisingly rich behavior of even the simplest configurations.

An excellent source for understanding thermal effects in space structures is Thornton’s *Thermal Structures for Aerospace Applications* [3]; along with overviews of the literature surrounding thermal control in airplanes and spacecraft, analytical and finite-element solutions to representative problems are derived and analyzed. This work provides the first step to analyzing thermal deformation of a boom – namely, the derivation of the steady-state temperature field under a radiant heat load; solving for this field is the first step in a multiphysics simulation, and so provides a useful check on any preliminary simulation results. Other works provide an insight into the deflection profiles of selected boom geometries, usually in the context of predicting thermal deflections of proposed or current spacecraft components. For example, Stohlman and Loper simulated the steady-state deflections of Triangular Rollable and Collapsible (TRAC) booms, including those used on The Planetary Society’s Lightsail-A, with some analysis of the effects of a vapor-deposited coating and a simulated composite with low coefficient of thermal expansion [4]. Stohlman also investigated the deflection of a cylindrical boom geometry in an analysis that coupled the heat transfer finite-element software Thermal Desktop with the dynamic finite-element software Abaqus, comparing the results to a previous analysis performed by Blandino [2, 5]. Chamberlain, Kiefer, and Banik also performed an analysis of cylindrical booms, analyzing the split-cylinder composite booms of the Air Force Research Laboratory’s Roll-Out Solar Array to determine the deflection and vibration modes induced by sunlight exposure under orbital conditions [6].

These studies provide insight into the potential magnitude of deflections a tape spring might experience, but as with many thin shells, the deflections and vibrations in question are very sensitive to the specific geometry of the boom; therefore, an analysis of tape springs in particular is helpful to understand the nature of the problem in general. A tape spring has bending stiffness orders of magnitude higher than that of an equivalently-sized flat tape while still being able to coil elastically around a hub. For small curvatures, an almost linear relationship exists with the bending moment, while for large curvatures (which cause the tape spring to buckle or “snap through”) the moment is constant at a much lower value [1]. The initial regime of small rotations, i.e. that of high bending stiffness, allows the boom to behave like a standard beam; the deflections investigated in our study are all of the small-curvature type.

\*Ph.D. Candidate, Graduate Aerospace Laboratories, 1200 E. California Blvd., Mail Code 250-45. pederson@caltech.edu

†Summer Undergraduate Research Fellow, Mechanical Engineering, 1200 E. California Blvd., Mail Code 104-6. aharaszti@caltech.edu

‡Joyce and Kent Kresa Professor of Aerospace and Civil Engineering, Jet Propulsion Laboratory Senior Research Scientist; Co-Director, Space-Based Solar Power Project, Graduate Aerospace Laboratories, 1200 E. California Blvd., Mail Code 105-50. AIAA Fellow. sergiop@caltech.edu

Modeling and predicting thermal deflections is the first step, albeit a challenging one. The difficulty mainly lies in the problem's inherently coupled nature: incoming heat flux on a boom causes a deflection, and the resulting deflection in turn changes the heating angle and resulting heat flux. In the case of sunlight, boom deflection causes a change in the local incidence angle of sunlight, which in turn changes the local heat flux and therefore the deflection; however, in front of a heat lamp, the deflection changes both the angle and intensity of the heat flux, since bending toward or away from the lamp shortens or lengthens the distance between the two.

Analytical models [?] give intuitive insights into the main parameters at play; accounting for conduction, radiation, and gain and loss of solar energy, these models offer a prediction of quasistatic and transient thermal effects for simple boom geometries (e.g. closed cylinders). However, when the factors of internal boom radiation, longitudinal conduction, any material anisotropy, or any geometric imperfection are considered, these models quickly become intractable and must be solved numerically.

Finite-element simulations offer a more powerful approach, able to account for virtually any of the above factors at the expense of computation time. For deflections of sufficient magnitude, the simulation must couple the thermal and mechanical analysis to ensure accurate results. Running these multiphysics, coupled, nonlinear simulations, which must account for solid mechanics of thin shells, heat transfer in shells, and radiative heat transfer at a bare minimum, requires significant computational power for any realistic deflection simulations.

Experiments offer the most direct means of measuring and observing real thermal deflections, but have their own limitations. Previous measurements of tape spring thermal deflections have used heat lamps or solar simulators to heat sample booms, usually under vacuum to prevent convective cooling [2, 3]. If space-like temperatures are simulated, the vacuum chamber and an interior shroud must be cooled using liquid nitrogen. The two conditions of vacuum and cryogenic temperatures are incompatible with most photogrammetry cameras and sensors, and thus make full-field measurements of displacement and temperature difficult. When these two conditions are even slightly relaxed – as they are in the experiments presented here – significant convective heat losses arise, which both reduce the temperature gradients and must also be accurately accounted for in any simulation verification.

We choose a geometry and a heating condition to experimentally replicate and simulate – namely, a thin-shell cylindrical section, or tape spring, and a radiative heat load shining perpendicular to the axis of the tape spring. This heat load causes thermal gradients to develop on the surface of the tape, which in turn create thermal expansion gradients that deform the structure; we therefore measure the deformation field and the temperature field as metrics of this thermoelasticity.

In this paper, we detail the development, performance, and results of an experimental rig that heats and measures a tape spring in this way, as well as those of a multiphysics simulation intended to replicate the experimental results. We then compare both results by means of deflection vs temperature plots, which reveal more complex behavior than the individual plots alone.

## II. Experiment

### A. Experiment Development

The apparatus used to measure temperature and deflection went through several iterations before arriving at the setup presented here; the various final choices are the result of various pitfalls and limitations of earlier setups.

Common across all of the apparatuses, however, were the four main components of 1) a tape spring sample mounted in a clamp, 2) an aluminum frame, 3) a steel baseplate, and 4) a quartz infrared heater (QIH) lamp hung parallel to the tape spring in the center of the baseplate. These components are schematically shown in Figure 1.

The tape spring samples were mounted in a "clamp", a  $0.5" \times 1.5" \times 1.5"$  aluminum block with two through-holes for  $1/4"$ -20 screws, using Epoxamite 103 epoxy resin with slow hardener. The aluminum frame,  $25\text{ cm} \times 30\text{ cm}$ , consisted of three extruded aluminum members bolted together in a post-and-lintel configuration, with the sample clamp bolted to the side of the lintel facing the heat lamp. The baseplate, to which the frame was bolted, was simply a  $18" \times 18" \times 0.5"$  steel plate with  $1/4"$ -20 threaded bolt holes every inch.

Initially, the sample, aluminum frame, and baseplate depicted in Figure 5(a) were mounted on a lab bench, with no separation from the surrounding air besides a thin black curtain (mostly for eye protection from the higher lamp power used in these initial tests). Temperature was measured in two ways: a thermocouple attached to the center of the tape spring, and a Teledyne FLIR thermal camera imaging the entire tape spring. Deflection was measured at a single point on the tip using a Keyence laser distance sensor. See Figure 2(a) and (b).

The unsealed, exposed nature of this setup was intended to help prevent any heat building up in the frame or the air

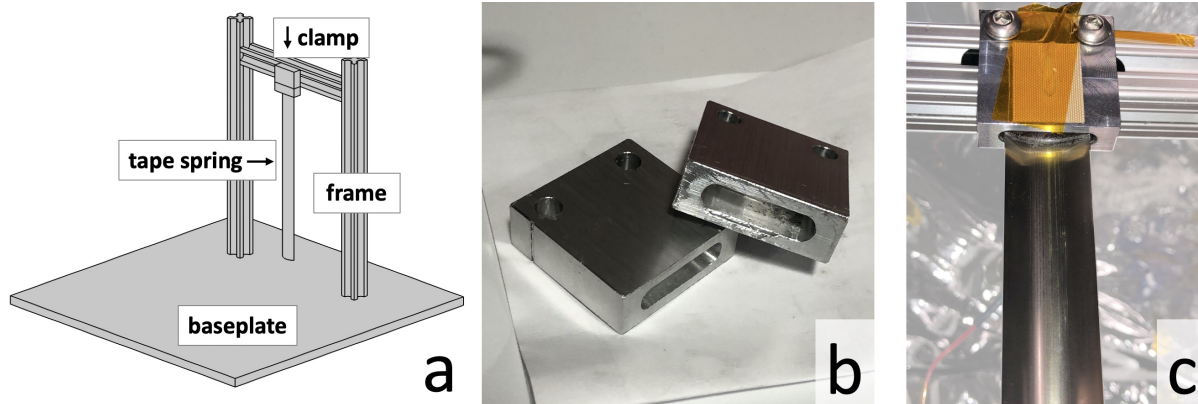


**Fig. 1** (a) The structural components common to all experimental setups: tape spring in "clamp", aluminum frame, and steel baseplate. The heat lamp (not shown) was placed in the center of the baseplate, parallel with the tape spring (b) A close-up of the aluminum "clamp", showing the pocket and bolt through-holes. (c) A close-up of the tape spring root, potted into the clamp and bolted to the aluminum frame. (Picture taken before applying paint speckles on thermocouple or root.)

surrounding the tape spring; this would hopefully prevent thermal expansions in any other part of the rig, while creating a much more predictable and stable temperature boundary condition for the simulation. However, preliminary tests revealed unexpected oscillation in the temperature readings, as shown in Figure 2(c). The period of these oscillations (seconds to minutes) was well above that of any structural oscillations on such a short tape spring and frame, suggesting a thermal nature; indeed, the problem was eventually revealed to be unpredictable air currents (such as those from an air conditioning system or people moving around the lab) randomly cooling the thin tape a few degrees. Even without random air currents, a consistent natural convection current cooled the tape spring, the heat loss of which was later predicted to be over a third of the total heat flux on the tape; this is obviously a large departure from replicating the intended environment, the vacuum of space. For both these reasons, then, it was decided to perform the next experiments in a vacuum chamber, where we could hopefully eliminate convection entirely.

As a next step, the same rig was mounted inside a large rectangular vacuum chamber at the Jet Propulsion Laboratory. The roughing pump alone was easily able to provide an atmosphere between 4-7 Pa during tests, which was predicted to reduce convection to 3% of its atmospheric value – more than enough for our purposes. The 43" × 32" × 22" chamber, despite having thick steel walls, allowed for tip deflection measurement in the same manner as the benchtop experiment: the sample tip was aligned with a quartz window mounted in one of the feedthrough ports, and the laser distance sensor "shot" through the window. See Figure 3(a) and (b) for a visual. Since thermal camera imagery was no longer possible in this setup, temperature readings were limited to thermocouples placed on the frame. Thermocouples placed directly on the tape were omitted for those tests to avoid affecting the tape mechanically or thermally.

Owing to the large reduction in convective heat loss, the temperatures reached in the JPL vacuum chamber were much higher than previous tests. After several tests with unpredictable deflections that were much larger than expected (see Figure 3(c)), a thermocouple was added to the tape spring, showing that the tape reached a temperature of 89°C. This temperature could have affected the potting epoxy, which had been cured at room temperature; as no other portion of the paint-stripped tape or clamp was sensitive to temperature (being metal), the outlier deflections were blamed on a delamination or additional curing of the epoxy mount. To correct this, later testing was performed at half or a quarter of the lamp power level used in the JPL tests (i.e. 25 W or 40 W, instead of 95 W).

## B. Final Experimental Setup

Learning from these previous test setups, a third and final experimental setup was constructed, consisting of the same steel tape spring clamped to an aluminum frame, in turn fixed to a steel baseplate, all contained within an acrylic thermal vacuum chamber. The setup is schematically shown in Fig. 4 for clarity. It also shows the positions of the thermocouples used to obtain temperature measurements, as well as the positions of the cameras used to obtain deflection measurements via Digital Image Correlation (DIC), both of which are detailed in Sections II.C and II.D.

The tape springs tested were sections of a Stanley PowerLock 33-425 tape measure, originally consisting of a 115

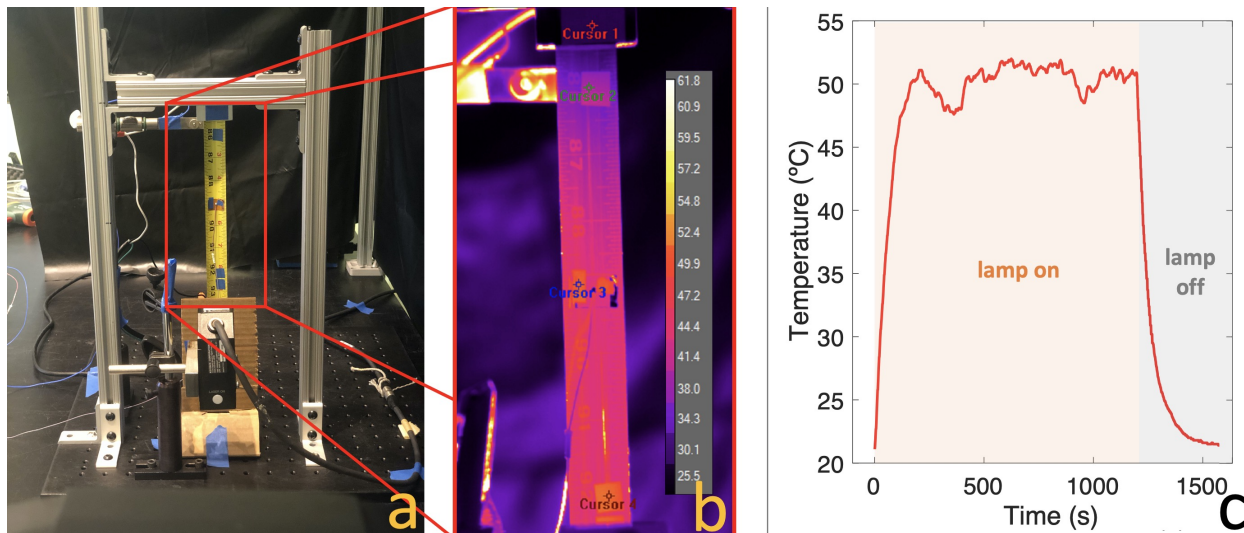


**Fig. 2** (a) A previous experimental setup, performed in air with no protection from air currents. Tape spring samples at the time did not have their original yellow paint removed. (b) An infrared image of the tape spring during a test, showing the qualitative temperature field. (c) The temperature output of the thermocouple attached to the tape, showing large thermal variations (at nominally steady-state) caused by air currents.

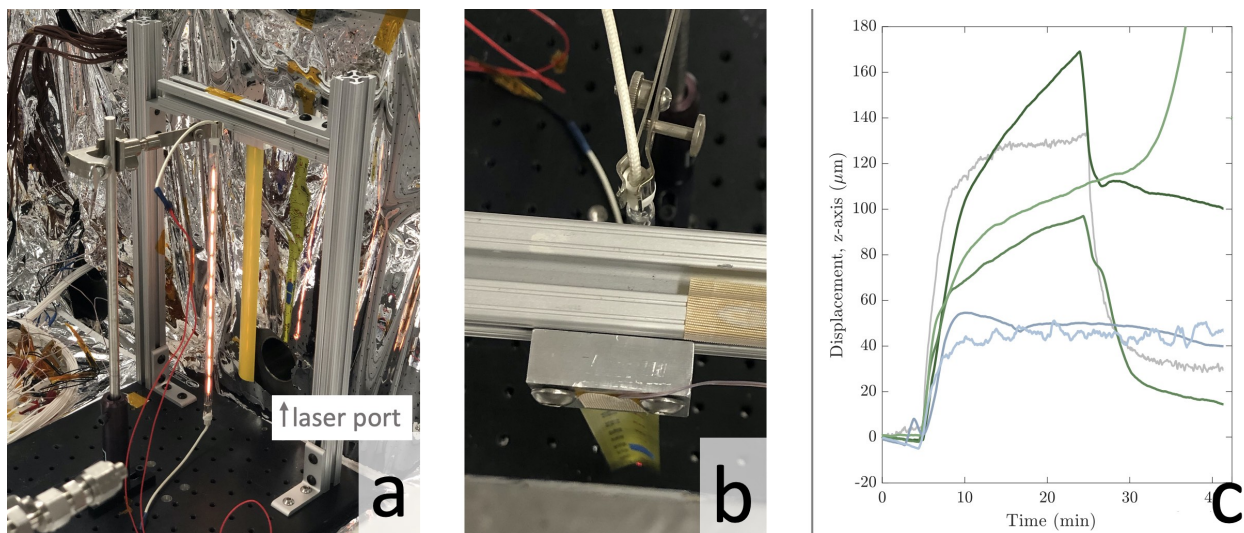


**Fig. 3** (a) Another previous experimental setup, performed in a large steel thermal vacuum chamber at JPL. Painted tape spring in the picture for visibility; the actual samples tested were stripped of their coating. The Keyence laser distance sensor "shoots" through the feedthrough window hole behind the tape tip. (b) The same tape from above, showing the glint of the laser dot pointed at the tip. (c) The deflection readings from various tests, showing wide variation in magnitude thought to be from potting epoxy overheating and potentially delaminating.

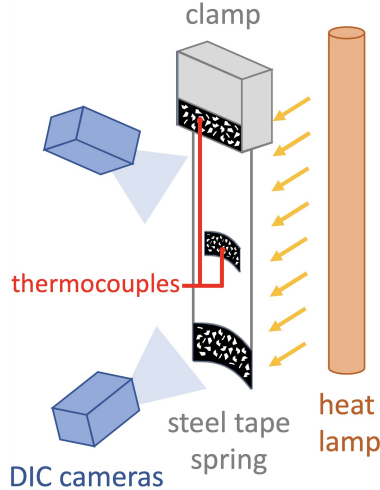


**Fig. 4** The experimental setup, cartooned with vertical axis not to scale. Note the placement of thermocouples on the middle of the tape spring and the clamp.

$\mu\text{m}$  thick piece of AISI 1095 high-carbon steel coated in yellow paint and a protective layer of Mylar. Immersing the tape springs in boiling water loosened the outer layer, enabling the paint and Mylar to be cleanly peeled from the samples. The samples were then potted into the aluminum clamp pocket using epoxy resin. After a 24-hour room temperature cure, the entire sample was baked in an oven at  $93^\circ\text{C}$  for an hour to raise the epoxy's thermal tolerance. White paint speckles were sprayed on the tip and root of the concave side previously coated with black spray paint, as well as on the two thermocouples mounted later. Finally, the clamp was screwed to the aluminum frame to cantilever downwards.

The tape spring length (25 cm) was chosen to ensure any dynamic effects were on a much shorter timescale than the heating of the boom, ensuring that the sample deflected according to a steady-state quasistatic response. The short boom length also ensured that the deflections predicted and ultimately measured were on the order of only  $100\ \mu\text{m}$ , similar to the thickness of the shell and much smaller than the sample length; these deflections are thus considered small, and the kinematics can therefore be linearized with almost no loss of prediction accuracy.

The tape was heated by a USHIO quartz infrared heater (QIH) lamp, hereafter referred to as the "heat lamp" or "lamp"\*. Since collimated sunlight is difficult to reproduce in the lab, the heat lamp was chosen as a more convenient heat flux source. It is worth noting that lamplight is not collimated like sunlight, and therefore falls off in intensity as the square of the distance from the lamp. While for large deflections (1-10 cm) this would cause the flux on the sample to change as the sample bent away from the lamp, the small deflections of our sample ( $10\text{-}100\ \mu\text{m}$ ) meant that this effect was negligible.

To heavily reduce convective heat losses, as well as eliminate measurement noise from small air currents, the entire experimental apparatus was mounted in a rectangular vacuum chamber (approximately 30" by 30" by 18") made of 1" thick clear acrylic walls — see Figure 5. Though a cylinder would be a more typical choice for a chamber form due to pressure loading, flat clear walls were a better candidate to perform DIC measurements.

The vacuum chamber walls were reinforced with additional acrylic struts on their exterior to prevent excessive bending when supporting external air pressure; see Figure 5(b). However, bending was not entirely eliminated; the refractive effects resulting from this bending required a more accurate calibration scheme, as described in Section II.E. Current limitations made the vacuum pressure achievable in the chamber around 5% atmosphere.

### C. Temperature Measurement

The vacuum chamber walls, being made of acrylic, actually block the band of infrared light used by forward-looking infrared (FLIR) thermal cameras; lacking the necessary feedthroughs and camera to operate in vacuum, a full-field temperature measurement was therefore impossible to achieve.

As a substitute, the tape spring and frame were instrumented with thin lightweight thermocouples to directly measure

\*The heat *lamp*, the source of the heat flux on the tape spring, is not to be confused with the LED *lights* used to illuminate the setup for DIC purposes.

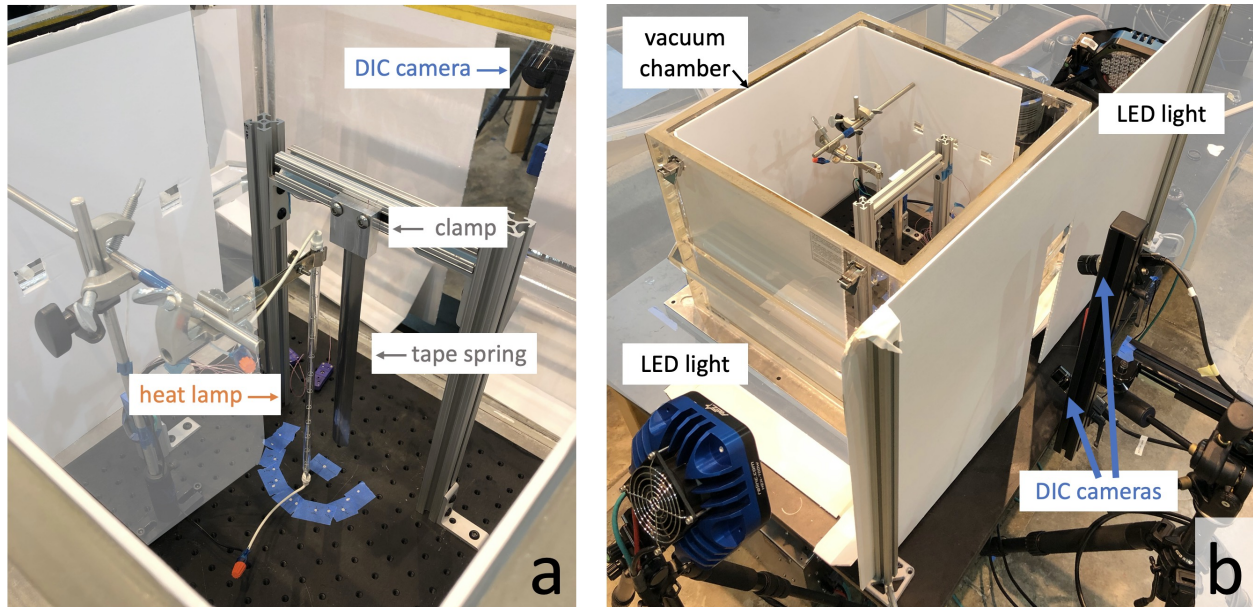


**Fig. 5** (a) The experimental setup in the acrylic vacuum chamber. Note the heat lamp and tape spring hanging vertically. (b) The same setup, zoomed out to reveal the LED lights and DIC cameras aimed through slits in the lightbox. Both views are missing the acrylic chamber lid and top lightbox panel for clarity.

surface temperature; the frame used an Omega fast-response type-E thermocouple with a polyimide adhesive pad (#SA1-E), while the tape spring used a similar model with a thin copper foil pad. Despite the obvious limitations and potentially invasive nature of the sensing, there was no other reliable and tested option for measuring the tape temperature. To be compatible with DIC, the backs of both thermocouple’s adhesive pads were speckled, allowing for the deflection precisely at the thermocouple location to be measured: see Figure 6(b) and Figure 7.

While the thermocouple placed on the clamp used a large standard adhesive pad, much care was taken to ensure that the thermocouple attached to the tape itself would affect the deflection as little as possible. Accordingly, the chosen thermocouple used only a thin adhesive copper foil to attach to the sample, trimmed to the smallest area that still avoided delamination: see Figure 7. In addition, the high-gauge thermocouple wire was carefully relieved of any prestrain and twisting, secured in such a way as to prevent exerting any bending or twisting force on the sample <sup>†</sup>.

#### D. Deflection Measurement via DIC

To obtain detailed displacement measurements before, during, and after heating, Digital Image Correlation (DIC) was used. Two digital cameras were mounted in the stereoscopic configuration needed to measure out-of-plane deflections, at a separation angle of approximately 40°; see Figure 6 for the placement of the cameras relative to the sample and chamber. The particular cameras used were Point Grey Grasshopper cameras GRAS-51S4M-C with a resolution of 2448 × 2048, 3.45 μm pixel size, and a gain range of 0 dB to 48 dB; both were fitted with 12 mm lenses, and both used an exposure time of around 6 ms.

To illuminate the sample, two RELInc WS3 LED lights were used at quarter power. To avoid DIC analysis errors caused by nonuniform illumination, shadowing of the tape spring, and glinting reflections, diffuse lighting was achieved with a lightbox of foam posterboard material constructed around and inside the vacuum chamber. The LED lights were then positioned such that their light entered from the lightbox sides and bounced off the front lightbox panel; the resulting light was sufficiently diffuse to eliminate any visibly nonuniform lighting.

The softwares VicSnap and Vic3D v9 were used to calibrate the rig, capture images during the test, analyze the images, and extract the resulting displacements. A subset size of around 30 pixels and a step size of around 4 pixels was used, adjusted in order to process the tip, thermocouple, root, and clamp speckled regions simultaneously.

<sup>†</sup>While the bending stiffness of the tape spring is much higher than that of the thermocouple wire, the *twisting* stiffness is comparable, making any residual forces applied by the thermocouple wire an important factor to consider. Carelessly securing the thermocouple wire to the frame was observed to visibly twist the sample.

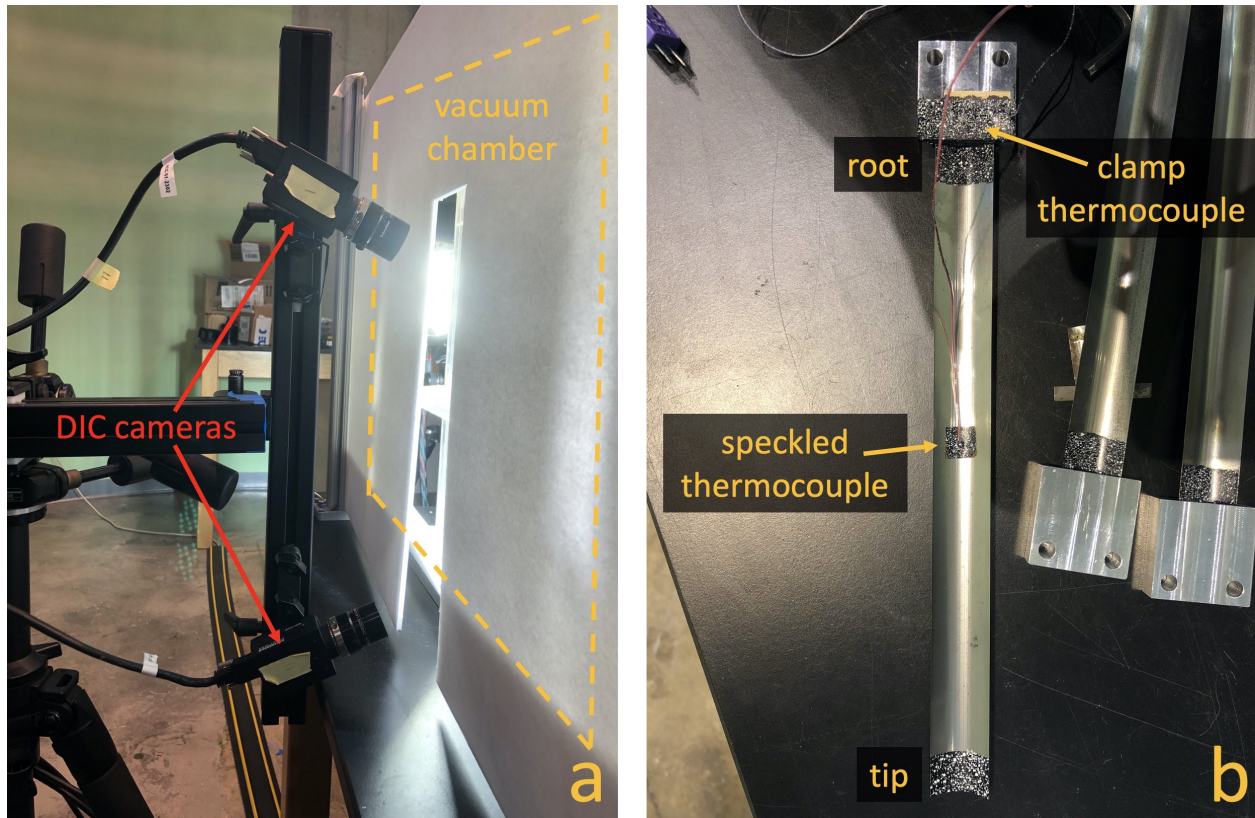


**Fig. 6** (a) The angle and distance of the DIC cameras relative to the vacuum chamber holding the experiment, with (b) a detail of a tape spring sample. Notice the position of the two thermocouples, the middle one being speckled for DIC measurements.

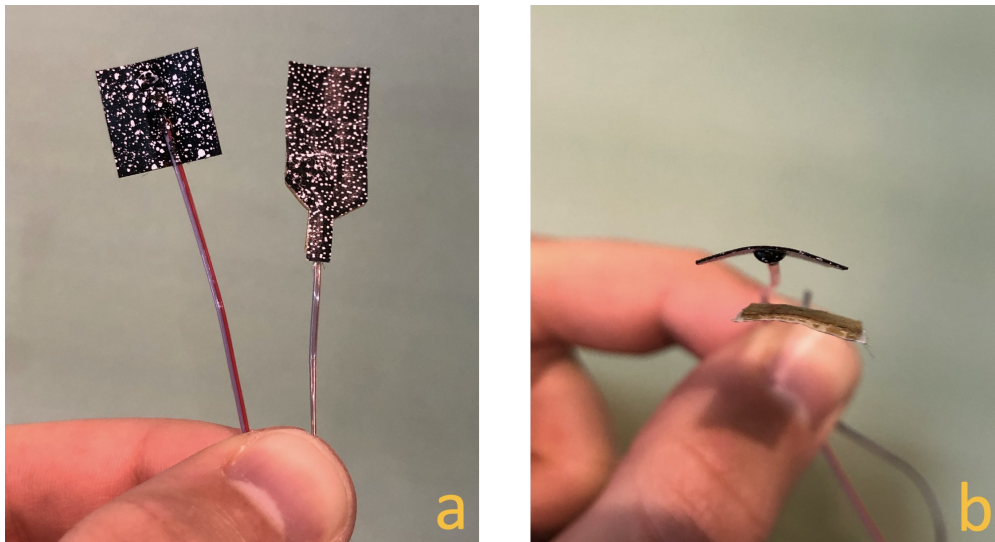


**Fig. 7** (a) The thermocouples affixed to the tape spring (left) and the clamp (right). (b) A detail of their relative thicknesses; note the thinness of the tape spring thermocouple pad and wire.

## E. Calibration Procedure

While calibrating the stereo rig is normally a straightforward task, the refractive effects and bending of the chamber walls required additional steps. When a straight, flat tape spring is viewed behind the thick acrylic wall, the residual curvature of the wall distorts the image of the tape spring, causing the "displacement" measurement of the tape spring to change by as much as 100  $\mu\text{m}$  at points. Even worse, when the chamber is supporting a vacuum, the walls curve inward even more, causing an additional distortion of this type. As these deflections are of similar or even *greater* magnitude than the heat-induced deflections we were attempting to measure, these erroneous refractive deflections had to be carefully accounted for and removed from the measurement to ensure accurate and trustworthy results. Accordingly, a calibration procedure was developed to accomplish this.

Since the rig could only be calibrated with the lid off (and therefore under no vacuum), the refractive distortion correction was performed in two steps: correcting the distortion caused by the chamber walls under atmospheric pressure, followed by the distortion under vacuum. To address the distortion caused by the residual curvature of the chamber walls under atmospheric pressure, a calibration using Variable Ray Origin (VRO) was implemented in Vic3Dv9; this consisted of a typical calibration using a calibration target, followed by a hybrid stereo calibration using a rigid speckled target. To address the additional distortion of the chamber walls under vacuum, DIC images were taken for five minutes under vacuum with the lamp still off, their erroneous deflection time-averaged, and then subtracted from the initial atmospheric state. This correction was then applied to all subsequent DIC images. These two error corrections, combined, gave deflection profiles that matched well with expectations based on previous experiments and simulations.

To examine the effects of the distortions in greater detail, as well as to confirm the effectiveness of the error-correction process, the tape spring samples were scanned with a FaroArm coordinate measuring machine. The resulting point cloud was then compared with the coordinates measured by DIC imaging of a fully-speckled tape spring in three configurations: outside of the chamber, inside of the chamber wall under no vacuum, and inside of the chamber wall under vacuum. Each of the DIC point clouds was aligned with the FaroArm point cloud in MATLAB and examined for discrepancies in the z-direction; Figure 8 shows all three comparisons. While the exact deviations in the z-coordinate were heavily sensitive to the exact alignment of the two point clouds, the overall shape and bowing of the tape spring remained readily observable; the DIC registered the tape as concavely bowed relative to the FaroArm data both outside of the chamber and in the chamber at normal pressure, but once the chamber was put under vacuum, the tape spring appeared convexly bowed. All of these uncorrected bowings were on the order of 100 microns, but the average deviation was an order of magnitude less, indicating an ability to accurately account for such refractive effects.

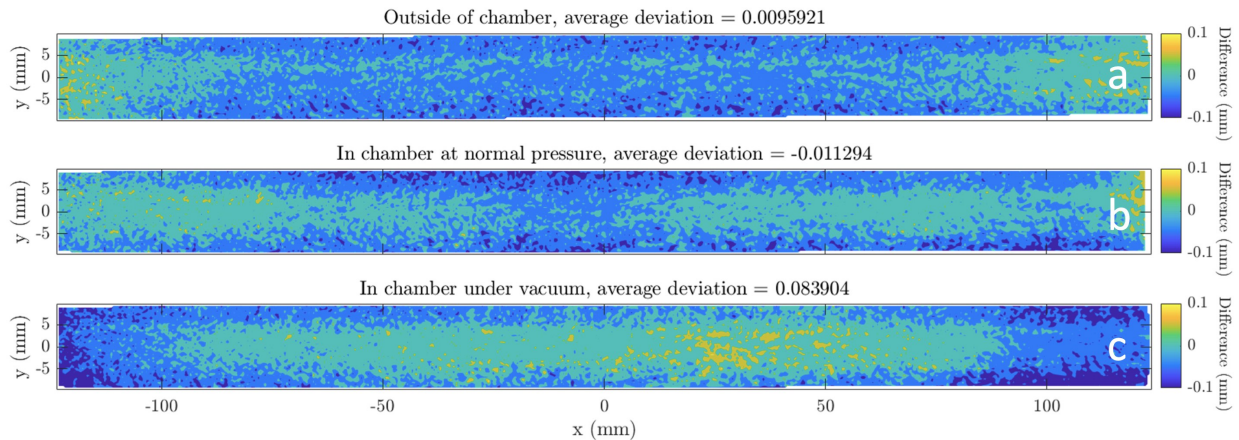


**Fig. 8** The comparison of the tape spring point clouds, measuring the approximate discrepancy in z-coordinate (in mm) between the FaroArm scan and the DIC measurement of the tape spring as positioned (a, top) outside the chamber, (b, middle) inside the chamber under no vacuum, and (c, bottom) inside the chamber under vacuum.

## F. Experimental Procedure

After potting, the tape spring sample was prepared for a test by applying white paint speckles to the clamp, root, and tip previously painted with black paint in order to get DIC measurements at those regions. The thermocouples were then placed on the clamp of the sample, as well as carefully placed on the desired location on the tape spring itself.

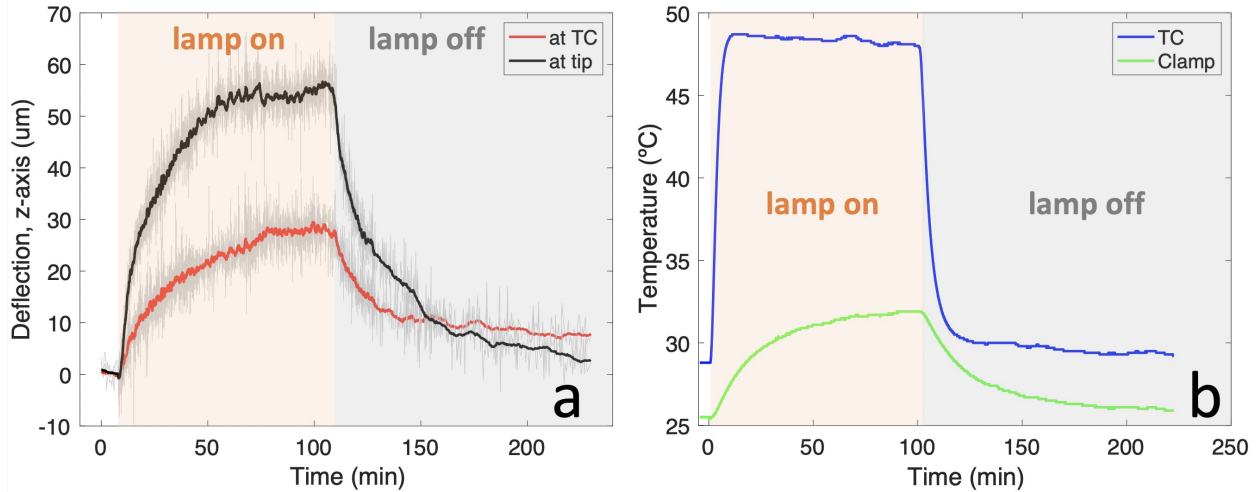


**Fig. 9** (a) Out-of-plane displacement of the tape tip and thermocouple (placed midway along its length) as extracted from DIC measurement, and (b) temperature of tape spring at the thermocouple and the clamp for a typical trial. Gray lines indicate raw data before moving window averaging, giving a sense of the measurement noise.

With the thermocouple reader logging temperatures of the tape and clamp the entire time, after calibration, five minutes of DIC images at 1 Hz were taken of the tape spring, in order to get the initial atmospheric state as mentioned above. The chamber was then subjected to 95 kPa of vacuum, and an additional five minutes of DIC images at 1 Hz were taken of the tape spring, in order to calculate the vacuum-distortion correction factor as above. The QIH lamp was then turned on, and the entire system was left to achieve a steady-state while DIC images were taken at rates between .03 and 1 Hz. Once a steady-state had been achieved – defined as the temperature changing less than 1° per hour and the deflection remaining proportionally steady – the QIH lamp was turned off, and the tape spring left to cool down until steady-state was reached again.

The DIC images were then processed to extract out-of-plane displacements, applying the error corrections described above to eliminate the refractive effects of atmospheric and vacuum-caused curvatures of the acrylic walls.

Over the course of testing, it became clear that with only around 3% of the lamp heat flux impinging on the tape spring, the rest of the setup and chamber was also heating significantly; this was confirmed with separate thermocouple measurements on the clamp, frame, and baseplate<sup>‡</sup>. Therefore, there was almost certainly additional thermal expansion of parts of the frame which would show up in the raw deflection reading of the thermocouple. To prevent any of these potential deformations from affecting the tape displacement measurement, the deflection and slope (i.e. tilt in the same plane as the out-of-plane deflection measured) at the clamp of the device were averaged, linearly fitted, and subtracted from the deflections measured on the tape itself. This yielded the tape deflection *relative to the clamp*, i.e. the deflection of an ideal experimental design with no deflection besides that of the tape.

A representative experimental result of both deflection and temperature measurements, used in the next section, is shown in Figure 9.

### G. Experimental Challenges

Placing a thin thermocouple on the sample itself, while having a negligible effect on the temperature distribution of the tape (as verified by simulation and hand calculation<sup>§</sup>), had a small twisting effect if anchored incorrectly. To minimize this effect, great care was taken in ensuring the thermocouple lead was anchored in such a way as to cause no torque on the sample.

A more serious problem lay in the thermocouple adhesive’s sensitivity to heat; the hotter the tape spring got, the more likely the contact adhesive would loosen and yield an incorrectly lower temperature reading during the later part

<sup>‡</sup>Frame temperature rises of 5°C weren’t uncommon during testing.

<sup>§</sup>The heat conducted by the thermocouple wire, assuming the highest thermally conductive properties, would be on the order of 0.05 W – two orders of magnitude lower than the power flux on the tape.

of a test. Over successive tests, the lamp power was reduced until this stopped occurring – namely at a lamp power of 25 W. This low power unfortunately had the side effect of taking much longer to reach a steady-state deflection; while the tape spring itself reaches a steady *temperature* within around ten minutes, the frame and surrounding chamber heat much more slowly under the small difference in heat. Therefore, the tape *deflection* takes a much longer time to stabilize, and did not appear to do so in several experimental trials, including the representative trial presented in these results.

In order to photograph the entire tape spring and clamp at once, and also maximize the DIC’s sensitivity to out-of-plane displacement, the DIC cameras had to be positioned at a sufficiently large incidence angle. Viewing the tape spring at such an angle meant the cameras needed a large depth of field to have the entire tape spring in focus, requiring a smaller aperture; this in turn required more light from the set of LED lamps. At the light levels required for the level of accuracy required, the entire chamber and testing rig would slowly heat to 8°C above room temperature; this waiting period and elevated resting temperature was accounted for in both simulation and data analysis.

### III. Simulation

A multiphysics finite-element simulation, performed using the software COMSOL, was compared with the experimental results. The entire experimental setup, including the tape spring, clamp, frame, baseplate, lamp, and chamber was modeled to ensure accurate conductive and radiative effects, as shown in Figure 12 (a).

The "Solid Mechanics of Shells" module, including a thermal expansion sub-module, was used to model the deflection of the tape spring, "Heat Transfer in Shells" modeled the heat transfer therein, and "Surface-to-Surface Radiation" modeled the heat flux of the heat lamp; a multiphysics module then coupled the radiation and heat transfer modules to complete the energy transfer. "Heat Transfer in Solids", "Heat Transfer in Solids", and "Surface-to-Surface Radiation" performed the same tasks for the clamp, frame, and baseplate, with the addition of a thermal expansion sub-module for the epoxy within the clamp<sup>¶</sup>. The mesh size was variable across the different components, but the tape spring used a mapped mesh with quad elements approximately 2 mm × 2 mm, i.e. 14 elements spanned the width of the tape spring. The values of the main geometric and material properties specified in the model are tabulated in Table 1.

The modules were solved for all the finite elements at each timestep; both "Stationary" (i.e. steady-state) and "Time-Dependent" (i.e. transient) analyses were performed using a linear analysis<sup>||</sup>. For the latter, a trial consisting of 100 minutes of the lamp on and 100 minutes of the lamp off was modeled; for the latter, the heat lamp source was disabled for the second half of the transient analysis.

**Table 1** Tape spring properties; material is AISI 1095 high-carbon steel.

Geometric		Material	
$L$	256 mm	$E$	205 GPa
$d$	30 mm	$\nu$	0.29
$R$	16.94 mm	$\rho$	7850 $\frac{kg}{m^3}$
$t$	0.115 mm	$k$	49.8 $\frac{W}{m \cdot K}$
		$C_p$	461 $\frac{J}{kg \cdot K}$
		$\alpha$ (CTE)	$11 \times 10^{-6} \frac{1}{K}$
		$\epsilon$ (emissivity)	0.9

#### A. Accounting for Convection

Despite the low pressures achieved in the vacuum chamber – 95 kPa of vacuum, or around 5% atmosphere – natural convection from residual air still conducted a significant amount of heat away from the tape spring<sup>\*\*</sup>. Correlations that predict heat loss due to natural convection based on sample dimensions and orientation are well-known in the heat

<sup>¶</sup>The thermal expansion of the epoxy within the clamp was found to have a non-negligible effect on the tape spring deflection, at least in simulation.

<sup>||</sup>Due to the aforementioned small deflections, both analyses were able to be run without requiring geometric nonlinearity, greatly reducing simulation time.

<sup>\*\*</sup>The relationship between convection and chamber pressure is nonlinear; from the calculation to follow, removing 95% of the air in the chamber only reduces convection by around a factor of four.

transfer community; for this analysis, the formulation for a vertical plate proposed by Churchill and Chu was chosen[7]. The prediction requires knowledge of the thermophysical properties of air (i.e. dynamic viscosity, density, thermal conductivity, etc.) at whatever pressure and temperature is present in the chamber <sup>††</sup>.

These air properties can in turn be predicted from chemical models of gases based on equations of state and other empirical measurements; such models have been collected by NIST to make a programming library called REFPROP [8]. This library is neither open-source nor free; however, a heavily-cited open-source equivalent using the same models is the library CoolProp, implemented in Python [9]. Given the air pressure and temperature, the library functions can calculate the thermophysical properties needed for the correlation; the correlation then provides a heat transfer coefficient,  $h$ , which is directly specified in COMSOL as an areal heat loss.  $h$  is calculated as

$$h = \frac{k}{L} \left( 0.68 + \frac{0.67 Ra_L^{1/4}}{(1 + (0.492/Pr)^{9/16})^{4/9}} \right), 10^{-1} < Ra_L < 10^9 \quad (1)$$

where  $L$  is the vertical length of the sample,  $k$  is the thermal conductivity of the surrounding air, and  $Ra_L$  is the Rayleigh number given by

$$Ra_L = \frac{g\beta}{\nu\alpha} (T_s - T_\infty) L^3 \quad (2)$$

where  $g$  is the gravitational acceleration,  $\beta$ ,  $\nu$ , and  $\alpha$  are the coefficient of thermal expansion, the kinematic viscosity, and thermal diffusivity of air,  $T_s$  is the average surface temperature of the tape spring,  $T_\infty$  is the average chamber air temperature, and  $Pr$  denotes the Prandtl number, the ratio of the kinematic viscosity and thermal diffusivity of air given by  $Pr = \frac{\nu}{\alpha}$ , all values being taken at the air pressure inside the chamber.

For our model tape spring, considering convection occurring on both sides of the tape, the natural convection heat transfer coefficient was calculated to be approximately  $2.48 \frac{W}{m^2 \cdot K}$ . Based on the amount of lamp power that directly impinged on the tape, the fraction of that heat lost to convection is therefore around 13%; this is much less than the atmospheric control, demonstrating the chamber's ability to heavily reduce (but not eliminate) the effect of convective heat loss.

## B. Other Thermal Considerations

Conductive heat losses from the tape spring via the clamp, as well as heat flow between the members of the aluminum frame crossbars, were also accounted for via COMSOL's default thermal contact model and verified with a simple 1D heat flow model.

The entire baseplate of the model was assumed to rest on a room temperature table in a room temperature lab; accordingly, the conductive heat boundary condition for the entire model lay in setting the underside of the baseplate to remain at room temperature throughout testing, even if the top of the baseplate was around 35° during testing. This may have been responsible for the room temperature reached by the simulation (and *not* the experiment) at "steady-state", as shown in the Results section, Figure 12.

The radiation boundary condition was similar. The walls of the acrylic chamber were assumed to remain at slightly above room temperature through the entire test, as they did in the experiment; therefore, all radiation heat loss from the tape spring and frame was to a sink slightly above room temperature. Note that the acrylic walls were modeled as purely radiative surfaces, having no mass or specific heat.

Prior simulations revealed the inadequacy of approximating the lamp flux as parallel rays from an infinitely far source; therefore the heat lamp was modeled by a collection of  $n$  point sources positioned at the correct distance away from the tape spring. It was found via iteration that  $n = 17$  point sources, each emitting 1/17 of the total lamp power, were able to mimic a finite heat source.

Steady-state and transient analyses were then performed, and after accurately accounting for the mentioned convective and conductive heat losses, the experimental temperature results were modeled to an at least qualitatively accurate degree. Fig. 10 shows the projected steady-state temperature profile of the tape spring.

---

<sup>††</sup> Even though these values change during the course of a test, the lamp was only lit when 95 kPa of vacuum had been reached, and the steady-state value of average tape temperature was known from experiment, meaning that we could simply calculate the value based on these steady-state quantities.

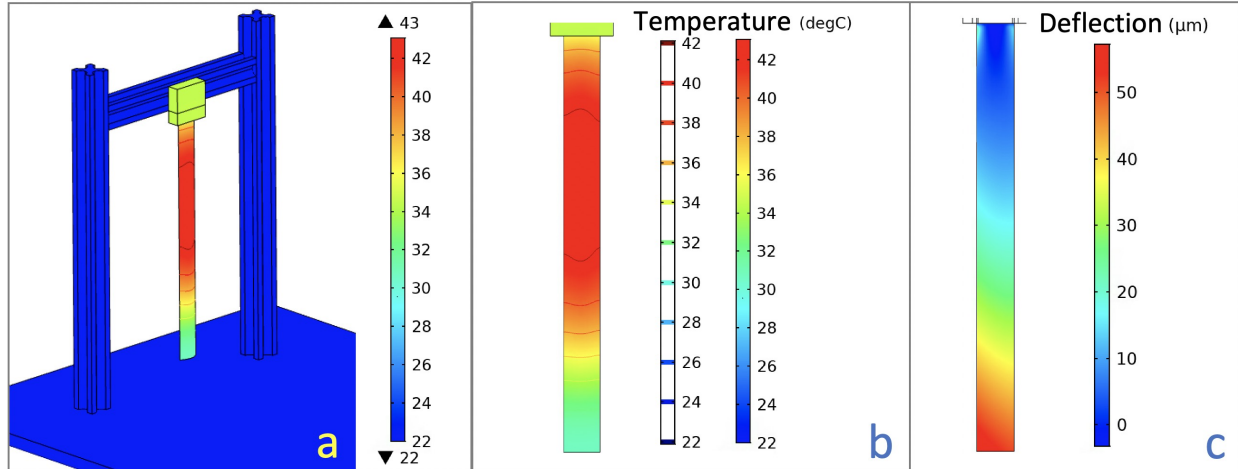


**Fig. 10** (a) The full COMSOL model of the experiment at a steady-state temperature (chamber walls hidden for clarity) with (b) a detail of the tape spring temperature profile (in °C) and (c) the deflection profile (in μm). Note the temperature gradient at the root and tip.

#### IV. Results and Discussion

The following plots contain time stamps indicated by  $t_0$  through  $t_8$ . These time stamps correspond to *events where something changes* in the experiment/simulation (e.g. the lamp turning off), or halfway points between such events. This is intended to facilitate comparisons across all the plots without regard to exact times.

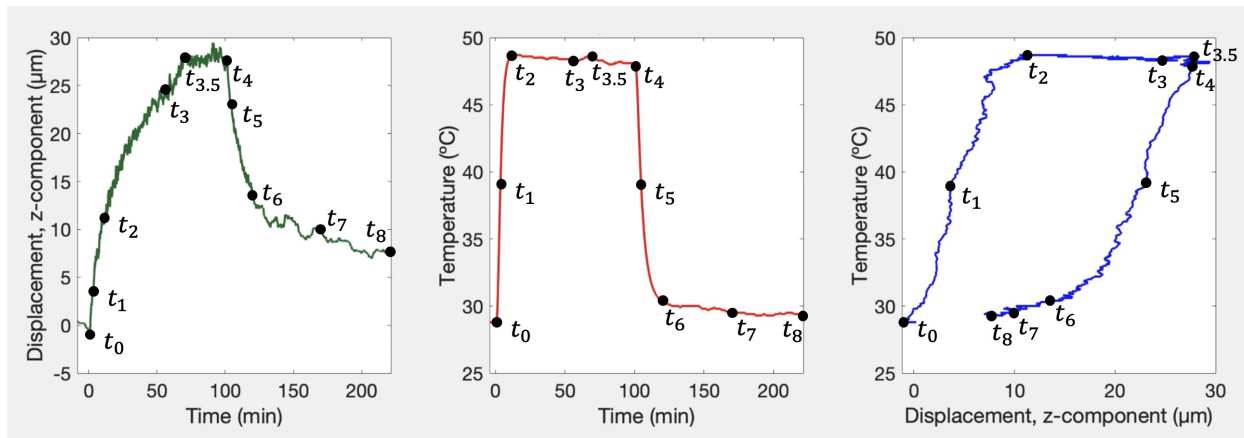


**Fig. 11** The thermocouple deflection vs. time (left), thermocouple temperature vs. time (center), and thermocouple deflection vs. thermocouple temperature (right) for the *experiment* tape spring. Corresponding times across all three plots marked with points  $t_0$  through  $t_8$ .

##### A. Experimental Results

The most obvious plots are shown in Figure 9 – tip displacement vs. time, thermocouple displacement vs. time, and the thermocouple temperatures vs. time. Plots of the thermocouple displacement vs. the thermocouple temperature alongside these two are shown in Figure 11.

As time increases from 0, a curve around the deflection vs. temperature curve begins at the lower left-hand corner, curves upward, slowly travels toward the upper-right for a bit, then curves down and leftward to the start in a clockwise direction.

We can observe that the curve does not trace a straight line, but has a "hysteretic" appearance; however, there is in fact no hysteresis occurring – see explanation below. However, we can observe that the tape quickly returns to the initial

temperature (vertical axis) and very nearly returns to the initial deflection after enough time has passed (horizontal axis). The points on the curve also show the relative rates of change of the temperature and deflection; the different spacing between points  $t_2$  and  $t_4$  vs points  $t_6$  and  $t_8$  show the difference in the speed at which the deflections are changing. Thus, the non-straight nature of this curve allows for a quick and easy visualization of how a test progressed over time.

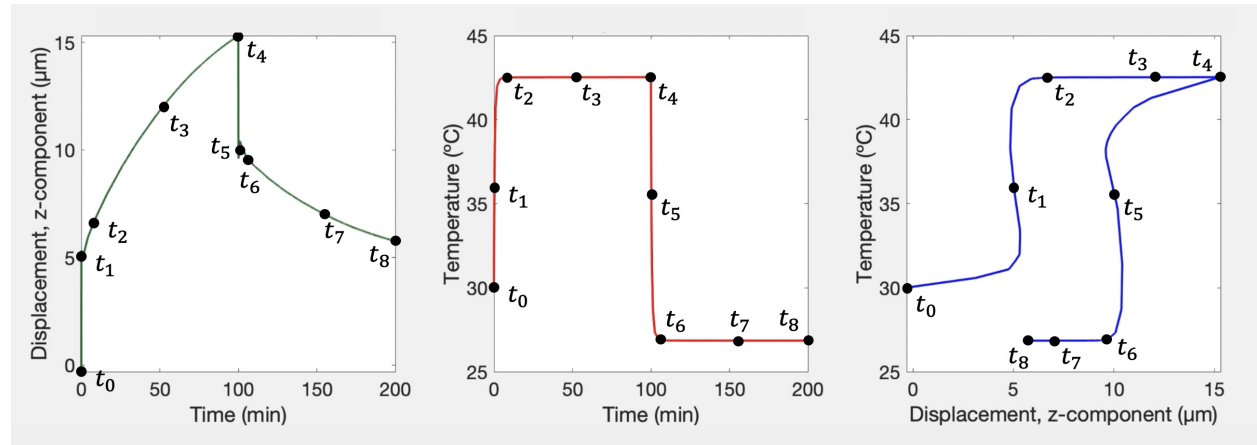


**Fig. 12** The mid-tape deflection vs. time (left), mid-tape temperature vs. time (center), and mid-tape deflection vs. mid-tape temperature (right) for the COMSOL tape spring model.

## B. COMSOL Results

Similar trends can be found in the results of the COMSOL transient simulation.

The COMSOL model reaches the point  $t_2$  roughly four times faster than the real experiment, suggesting a difference in thermal conductivity either somewhere in the frame or baseplate. While the simulation would take a prohibitively large amount of computational time to reach a true steady state, the initial heating period shows a similar trend to the experimental data, even replicating the clockwise loop.

An interesting observation lies in the dropping of the COMSOL "steady-state" temperature to *below* that of the initial conditions. As mentioned in the Simulation section, the baseplate was assumed to rest on a room-temperature table in a room-temperature lab, just like the experimental one; however, the simulation did in fact reach that steady-state, while the experimental rig did not. This is almost certainly due to the lack of modeling of the acrylic walls as solid objects; in modeling them as radiative surfaces alone, they were not able to absorb lamp heat during the test and thus supply the baseplate with any heat when the lamp was turned off.

As for the S-shaped nature of the COMSOL curves, they would be the result of deflection changing faster than expected when the lamp was turned off or on. The lamp was turned on or off instantaneously in the COMSOL model, while in reality the lamp took at least 1.5 s to heat up and 10 minutes to fully cool off (as was later measured by a FLIR camera). This would slightly slow the change of temperature for the experiment, potentially removing this effect. Incorporating the finite lamp illumination time (perhaps by ramping the lamp power with a linear approximation) would be an interesting part of future simulations.

## C. Explanation of "Hysteretic" Curves

An explanation of the hysteretic shape of these curves requires a small detour into the nature of the transient temperature field. (The transient *deflection* field is a direct result of the transient temperature field, so we will focus on the latter.)

As a contrasting example, consider a beam, clamped at one end, with a point load  $P$  at the tip; the point load varies as a function of time, and the tip deflection  $w$  and the moment at the root  $M$  are dependent variables. For simplicity, we will only consider the quasistatic case – i.e. we will neglect any dynamic effects. Since the moment is the product of the point load times the cantilever length ( $M = P(t)L$ ), and the deflection is  $w = \frac{P(t)L^3}{2EI}$ , plotting  $M$  vs  $w$  would yield a straight line, with different values of  $P$  falling on that line. Note that the curve would enclose no area; this is because each point load results in a unique  $w$  and  $M$  independent of time.

This means that the solution can be decomposed into a spatially-varying function (i.e. a function purely of  $x$ , the position along the beam) and a time-varying function (i.e. one purely dependent on time); in other words, the “shape” of the deflection is independent of the time history that produced it. Therefore, the function of  $t$  is able to be separated from the rest of the solution. It is also helpful to think of the time-independence as resulting from the linear nature of the loading and response: for small deflections, the beam behaves as a linear spring, with a linear increase in point load resulting in a linear increase in tip deflection.

This would also be the expectation for a simple system responding to a temperature change; for example, uniform heating of a solid one-dimensional bar would result in a one-to-one relationship between bar temperature and axial thermal expansion in much the same manner.

This lies in direct contrast to the temperature response to the heating of a tape spring. The heat load can be considered as approximately uniform (i.e. linear along the length with a slope of zero), and the conductive heat loss, without any convection or radiation to cool it, from Fourier’s Law would result in a linear drop in temperature from a maximum at the tip to the boundary temperature at the root (i.e. a linear function of  $x$  along the length). However, convection and radiation both involve nonlinear functions of temperature, meaning that the responses are not path-dependent. This results in a time-dependent “shape function” of temperature, one that changes with time based on the set of initial conditions that produced it.

Indeed, the deflection at any point on the tape spring is an integrated combination of the thermally induced deformation from the root to the point in question, meaning that there is an infinite number of temperature fields that could yield a certain deflection – even while the measured thermocouple temperature remains the same. Which one of these fields appears on the tape spring is a function of the time and the heating conditions of the boom. Suddenly turning the heat lamp on from a steady-state of being off is one of these heat conditions; suddenly turning the heat lamp off from a steady-state of being on is another. These conditions cause two different paths to be followed by the deflection vs. temperature response: the first on the way up, and the second on the way down. Thus, a hysteretic path shape is created, even though there is no energy loss in this process.

## V. Conclusions and Future Work

From seemingly simple experiments involving heating a steel tape spring and comparing the results with multiphysics simulations, we have characterized a rich set of deflections and thermal behaviors, involving apparent hysteretic behavior. These observations yielded insights into the temperature profiles of a thermally loaded boom, as well as potentially unexpected deflection behavior.

Characterizing the full-field deflection of the tape spring experimentally did in fact help confirm previous simulation predictions. A direct observation of the variation of deflection of various points along the tape spring, accomplished via DIC, permitted more accurate assessments of the relations only hinted at by previous predictions.

The series of experimental setups leading to the current one gave insight into the various factors that make replication of heat-flux-driven bending on Earth challenging, while the current setup still leaves areas for improvement. Many factors contributed to the difficulty of the setup to reach a steady-state, including lack of contact-free thermal measurement, incorporation of epoxy, and even the illumination needed for DIC measurements. These will be addressed in future experimental setups.

Testing in vacuum unfortunately only partially eliminated a large modeling uncertainty. The heat flux leaving the tape spring via convection was calculated to be around 13% of the total heat leaving the tape spring; this value would ideally be much lower for results that would more effectively mimic the space environment.

The heating of the tape spring in these experiments was always introduced perpendicular to the axis of the tape spring; rotating the tape spring about its axis (or equivalently, revolving the lamp) will induce different, non-symmetric temperature profiles, as well as the possibility of twisting (a circumstance carefully avoided in the tests presented here). A more comprehensive survey of these effects, performed in an experimental rig free of the various limiting factors herein described, will be the focus of continuing research.

Finally, the simulations involved are being further improved, and have even helped improve the experimental rig. For example, a large source of modeling uncertainty lay in the relatively large aluminum frame holding the tape spring; being the same distance from the lamp, it also heated up, but due to the large variance of emissivity with surface finish, the amount of heat absorbed was difficult to predict, even with thermocouple data at certain points. In addition, every bolt and connection in the frame constituted a thermal contact whose thermal conductance is not fully known. While reasonable results were achieved after much iteration, it would be ideal to have a setup in which these unknown connections were minimized or absent.

## Acknowledgments

The authors would like to thank Eric Sunada, Lead Thermal Technologist in Propulsion, Thermal, and Materials Systems at the Jet Propulsion Laboratory, for his invaluable insight on thermal experiments and modeling. The National Science Foundation's Graduate Research Fellowship Program, the Caltech Space Solar Power Project, and the Caltech Summer Undergraduate Research Fellowship program provided financial support for this research.

## References

- [1] Miura, K., and Pellegrino, S., *Forms and Concepts for Lightweight Structures*, 1<sup>st</sup> ed., Cambridge University Press, UK, 2020, Chap. 8.
- [2] Stohlman, O. R., "Coupled radiative thermal and nonlinear stress analysis for thermal deformation in large space structures," *5th AIAA Spacecraft Structures Conference*, 2018. <https://doi.org/10.2514/6.2018-0448>.
- [3] Thornton, E. A., *Thermal Structures for Aerospace Applications*, 1<sup>st</sup> ed., American Institute of Aeronautics and Astronautics, 1996, Chaps. 4, 9.
- [4] Stohlman, O. R., and Loper, E., "Thermal deformation of very slender TRAC booms," *3rd AIAA Spacecraft Structures Conference*, 2016. <https://doi.org/10.2514/6.2016-1469>.
- [5] Blandino, J. R., "Analysis of thermal-mechanical interactions of STEM booms," *2nd AIAA Spacecraft Structures Conference*, 2015. <https://doi.org/10.2514/6.2015-1164>.
- [6] Chamberlain, M. K., Kiefer, S. H., and Banik, J., "On-orbit structural dynamics performance of the roll-out solar array," *5th AIAA Spacecraft Structures Conference*, 2018. <https://doi.org/10.2514/6.2018-1942>.
- [7] Churchill, S. W., and Chu, H. H. S., "Correlating equations for laminar and turbulent free convection from a vertical plate," *International Journal of Heat and Mass Transfer*, Vol. 18, No. 11, 1975, pp. 1323–1329. [https://doi.org/10.1016/0017-9310\(75\)90243-4](https://doi.org/10.1016/0017-9310(75)90243-4).
- [8] Huber, M. L., Lemmon, E. W., Bell, I. H., and McLinden, M. O., "The NIST REFPROP Database for Highly Accurate Properties of Industrially Important Fluids," *Ind. Eng. Chem. Res.*, Vol. 61, No. 42, 2022, p. 15449–15472. <https://doi.org/10.1021/acs.iecr.2c01427>.
- [9] Bell, I. H., Wronski, J., Quoilin, S., and Lemort, V., "Pure and Pseudo-pure Fluid Thermophysical Property Evaluation and the Open-Source Thermophysical Property Library CoolProp," *Ind. Eng. Chem. Res.*, Vol. 53, No. 6, 2014, p. 2498–2508. <https://doi.org/10.1021/ie4033999>.